Surface & Coatings Technology 232 (2013) 747–757

Contents lists available at ScienceDirect

Surface & Coatings Technology

journal homepage: www.elsevier.com/locate/surfcoat

Application of resonant ultrasound spectroscopy to determine elastic constants of plasma-sprayed coatings with high internal friction

Pavel Sedmák [a], Hanuš Seiner [b,*], Petr Sedlák [b], Michal Landa [b], Radek Mušálek [c], Jiří Matějíček [c]

[a] Faculty of Nuclear Sciences and Physical Engineering, Czech Technical University in Prague, Trojanova 13, 12000 Prague, Czech Republic
[b] Institute of Thermomechanics, Academy of Sciences of the Czech Republic, Dolejškova 5, 18200 Prague, Czech Republic
[c] Institute of Plasma Physics, Academy of Sciences of the Czech Republic, Za Slovankou 3, 182 21 Prague 8, Czech Republic

ARTICLE INFO

Article history:
Received 13 February 2013
Accepted in revised form 20 June 2013
Available online 29 June 2013

Keywords:
Plasma-sprayed coatings
Elastic constants
Resonant ultrasound spectroscopy
Internal friction
Anisotropy

ABSTRACT

We present a novel modification of resonant ultrasound spectroscopy (RUS) for analysis of elastic constants of plasma-sprayed coatings in the 'as sprayed' state, i.e. without removing the substrate. This modification is suitable for coatings with high internal friction ($Q^{-1} \gtrsim 10^{-2}$), which cannot be measured by RUS in the free-standing state due to strong damping. In combination with through-transmission measurements, this modification is able to provide full anisotropic tensor of elastic constants of the coating. As an illustrative example, the proposed methodology is applied to two steel coatings prepared by water-stabilized plasma (WSP) spraying. In addition to the moduli, also the internal friction parameters of the coatings are obtained. The results of RUS are compared to moduli determined by four-point bending tests, and it is shown that the anisotropic elasticity of both examined materials exhibits an elliptic form of transversal isotropy with four independent elastic coefficients.

1. Introduction

Elastic moduli are among the key parameters of surface coatings prepared by thermal spraying. Not only they are direct indicators of porosity and integrity of the coating, i.e. of the quality of mutual bonding of the splats [1,2], which makes them usable for adjustment of technological parameters of the spraying. Their exact knowledge is also essential for estimation of residual stresses arising due to quenching of the droplets and thermal expansion mismatch between the substrate and the coating [3–5], or stresses induced by elastic straining of the underlying substrate. From the latter point of view, the in-plane elastic constants are of the highest importance, as the mechanical loads imposed into the surface layer by the strain field of the substrate are, providing that the thickness of the coating is small, predominantly of in-plane nature. Lastly, the elastic moduli of the coating are basic input parameters necessary for numerical (e.g. FEM) modeling of coated bodies and their reliable knowledge is for such computations substantial.

For plasma sprayed coatings, the elastic moduli are most usually determined by micro- or nano-indentation [6–8]. This method has many advantages, providing for example some insight into the anisotropy of the coating [2,6]; the nano-indentation can be also used for mapping of the moduli across the coating microstructure [9]. On the other hand, the stresses applied on the coating during the indentation are locally very high, usually above the yield limit of the material but limiting to zero with increasing distance from the indentation point. Hence, due to the well-known strongly non-linear character of the elastic behavior of the plasma-sprayed coatings [10], it is not exactly clear which stress level the obtained elastic constants correspond to. Another undesirable feature of the indentation method is the strong dependence of the measured elastic modulus on the indentation depth and load-influenced volume [7,11].

For these reasons, alternative methods working with lower and better defined stress levels are often employed, ranging from classical (static and dynamic) tensile and bending tests [12–15] to neutron scattering [16], X-ray diffraction [17] and ultrasonic methods. A wide variety of ultrasonic techniques has been successfully applied for this purpose so far, including contact measurements of velocities of bulk and surface acoustic waves [18–20], immersion methods [21], laser-based ultrasound [22] and Brillouin scattering [23]. The main motivation for the use of these methods is that the level of strain oscillations carried by the ultrasonic waves is extremely low ($\sim 10^{-6}$, which is e.g. by two orders of magnitude lower than in typical four-point bending tests), so a purely linear elastic response is obtained without inducing any damage to the material.

Most recently, Tan et al. [24] have applied resonant ultrasound spectroscopy (RUS, [25,26]) to determine elastic constants of free-standing coatings prepared by atmospheric plasma spraying (APS) and high-velocity oxygen-fuel (HVOF)process. RUS is an advanced ultrasonic method based on determination of the elastic moduli from resonant spectra of free elastic vibrations of a small sample of the examined material. This approach seems to be very promising,

* Corresponding author. Tel.: +420 266053712.
E-mail address: hseiner@it.cas.cz (H. Seiner).

0257-8972/$ – see front matter © 2013 Elsevier B.V. All rights reserved.
http://dx.doi.org/10.1016/j.surfcoat.2013.06.091

since the RUS method works with wavelengths comparable to the dimensions of the samples (few millimeters), which are incomparably larger than any characteristic length-scales of the microstructure (dimensions of splats, pores and cracks). The resulting elastic constants can be therefore expected to describe well the macroscopic (homogenized), purely elastic behavior of the coating. Moreover, if the used samples are thin plates (as in the case of Tan et al. [24]), the majority of the vibrational modes are bending modes, so the RUS measurement is particularly sensitive to the bending stiffnesses of the sample, which are closely related to the in-plane elastic moduli.

Nevertheless, the RUS method is applicable only for coatings with acceptably low internal friction, for which the sample can be set into resonance and individual resonant peaks in the spectrum can be easily distinguished. For some plasma sprayed coatings, however, the typical values of the internal friction are relatively high ($Q^{-1} \sim 10^{-2}$, [27]) due to their somehow loose microstructure that is desirable e.g. for enhanced strain and thermal shock tolerance of the coating. Such high value of Q^{-1} may result in problems both in generation of the vibrations (higher energy of the generating pulses is needed) and in identification of resonant peaks (the broadened peaks are overlapping and the signal-to-noise ratio is decreased). In this paper, we present a modification of RUS method for the analysis of supported coatings instead of the free-standing ones. In such case, i.e. if the sample for RUS consists of a thick substrate with a significantly thinner coating deposited on it, the resultant resonant spectrum is mainly the spectrum of the substrate, with the individual peaks only slightly shifted by the presence of the coating. Similarly, the high internal friction in the coating leads only to limited broadening of the individual resonant peaks, so the identification of the resonant frequencies is still possible, and the sample itself can be easily set into resonance.

This modified approach originates from classical RUS method for evaluation of thin layers [26,28], which is based on the comparison of the resonant spectra of the same substrate sample before and after deposition of the layer. The shifts of the peaks then carry information on the in-plane elasticity of the layer. In a similar manner, in this paper we obtain an information on the in-plane elasticity of the coating by analysis of the evolution of the spectrum of one sample during subsequent removal of the coating by grinding (as described in details in Section 3.1.). We show that such analysis is possible even if the spectra are significantly damped (internal friction of the coating $\gtrsim 10^{-2}$), and, when complemented by classical through-transmission measurements, this approach enables determination of the full anisotropic tensor of the elastic constants. Moreover, from the shifting and broadening of the peaks with increasing thickness of the coating, additional information on the coating can be extracted, which we employ in this paper for the determination of the internal friction parameters. In summary, the experimental technique proposed in this paper differs from the conventional RUS method in two points: (i) the measurements are carried out on heterogeneous, sandwich-like samples consisting of a substrate (known material with low internal friction) and thick layer of the coating (unknown, highly dissipative material); (ii) the measurements are repeated with several successive removals of the coating material, so the dependence of the resonant spectrum on the thickness of the coating is obtained and used for inverse calculation of the elastic constants of the coating.

A similar approach to the one presented in this paper was also developed by Lauwagie et al. [29], who determined in-plane moduli of air-plasma sprayed thermal barrier coatings (TBC) from resonant spectra of small bars including both the substrate material and the coatings. Lauwagie et al. [29] used a finite element code for the calculation of resonant frequencies of such samples and obtained the resulting elastic constants by tuning the input parameters of this code until an optimal fit was reached. Unlike the approach reported in [29], our method is comparative: it extracts the information on the elastic moduli of the coating from the differences between the spectra of the substrate with and without the coating. This ensures that our results are much less influenced by the uncertainties in the knowledge of the properties of the substrate itself. Moreover, fitting the whole evolution of the spectrum with successive removals of the surface layers enables a deeper insight into the structure of the coating, and, as also shown in this paper, the estimation of the effective location of the roughened substrate-coating interface. On the other hand, the method described in this paper is destructive: the coating is fully removed after the measurement.

2. Materials under study

Two stainless steel coatings with different volume fractions of oxides were chosen for the RUS analysis in order to observe if the proposed RUS method will show the expected difference in the stiffness of these coatings. Both these coatings were sprayed onto common low carbon steel substrates from a 316L powder of nominally 106–150 μm size range (Stamont International, Slovakia) using a water stabilized plasma (WSP) torch (Institute of Plasma Physics, ASCR, Czech Republic) with the following parameters used: torch power 160 kW, powder feeding distance 100 mm, and powder feed rate 270 $g \cdot min^{-1}$. In both cases, the coating thickness was approximately 1 mm and the substrate thickness was 2.5 mm (lateral dimension 25 × 100 mm). The difference in the content of oxides was deliberately induced by different spraying distances (as a consequence of interaction of the flying molten droplets with a surrounding atmosphere): one of the coatings was deposited at distance of 300 mm, and the second at distance of 500 mm. Oxygen content in the coatings was determined by electron probe microanalysis (EPMA) in a Camscan 4DV scanning electron microscope with a Link AN1000 (Link Analytical, UK) analytical system. The volumetric percentage of the oxide phases was determined by image analysis of the SEM images of polished cross sections. The results were as follows: the coating deposited at 300 mm spraying distance contained 2.72 wt.% (11 vol.%) of oxides and will be hereafter referred to as the LO (low oxides) coating; the coating deposited at 500 mm spraying distance contained 7.65 wt.% (20 vol.%) of oxides and will be hereafter referred to as the HO (high oxides) coating. SEM micrographs of the coatings under study and of the substrate-coating interfaces are given in Fig. 1.

Preliminary estimations of the in-plane Young's moduli of these two coatings were obtained by four-point bending (4 PB) tests. This was done in an Instron 1362 universal testing machine (Instron, UK). The coatings were tested in the as sprayed condition (on substrates) and loaded in compression up to a small strain of 0.05% to minimize the structural damage. The substrate and coating contributions to the total stiffness were separated according to [30]. The result was that $E_{HO} = (45 \pm 9)$ GPa and $E_{LO} = (28 \pm 7)$ GPa, where the subscripts LO and HO correspond to the denotation of the respective coatings.

From each of the examined materials, a rectangular parallelepiped sample for the RUS measurements was cut, containing both the coating and the underlying substrate and with top and bottom faces parallel to the substrate-coating interface. As explained in the Introduction section, the applied modification of RUS required the coating to be significantly thinner than the substrate, which was not fulfilled for the initial thicknesses of the coatings. For this reason, a part of the coating was removed prior to the RUS measurements by grinding, until the ratio between the thickness of the substrate and of the coating higher than 5:1 (about 2 mm of the substrate to 400 μm of the coating) was reached. After this first partial removal of the coating, all faces of the samples were ground and polished to ensure plan parallelism of the opposing faces. Final dimensions of the two resulting samples are listed in Table 1 (in agreement with this table, we will from hereafter use the denotation a for the thickness of the sample in the direction perpendicular to the substrate-coating interface.)

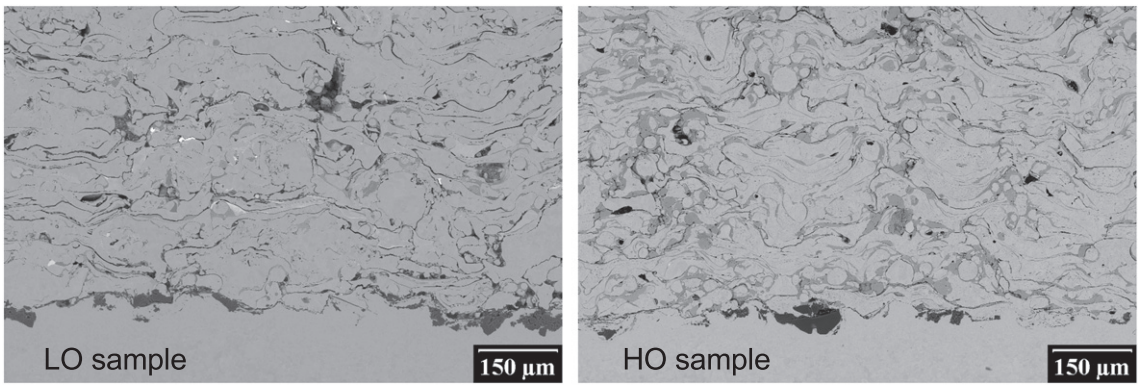

Fig. 1. SEM micrographs of the two coatings under study. Close to the bottom edge of each micrograph a wavy (grit-blasted) substrate-coating interface with embedded grit-blasting particles can be seen.

3. Modified RUS method

3.1. Experimental procedure

The resonant spectra of free elastic vibrations of both samples were measured by the contact-less RUS technique [31,32], with the vibrations both generated and detected by lasers (see [31,33] for instrumentation and further details and Fig. 2 for a schematic outline of the experimental set-up), and with the modal shapes recorded by laser-Doppler interferometry. The out-of-plane component of the displacement field was measured in a 20 × 20 mesh of points covering equidistantly the largest face of the sample, which enabled the reconstruction of the projections of the modal shapes onto this face, as usual in mode-sensitive RUS measurements. The spectra were obtained in frequency range 200 kHz–2 MHz. Due to the strong damping of the coating, the quality factor of the obtained spectra was rather low, enabling only few resonant peaks (10 for the HO Sample and 8 for the LO Sample) to be reliably detected and identified based on the modal shapes.

After this first step, a thin upper layer of the coating was removed by grinding for each sample, and the spectra were remeasured. As the thickness of the coating was decreased by the grinding, the resulting spectra were less damped and enabled detection and identification of a higher number of resonant frequencies. This procedure was repeated three times, with the thickness of the surface layer removed in each step being always between 50 μm and 100 μm. Then a slightly thicker layer (>150 μm) was removed to grind out fully the surface-coating interface (the fourth repetition). Finally, again a layer thinner than 100 μm was removed (the fifth repetition). The exact values of the dimension *a* after the individual grindings are given in Table 2.

After the fourth grinding, the coating was already fully removed, which means that the last two spectra (after the fourth and the fifth repetition) corresponded to the samples containing only the substrate materials. Thus, for each sample, the evolution of the identified modes with the decreasing thickness was obtained both for the substrate-layer system and for the substrate itself. An example of such evolution is shown in Fig. 3, where selected parts of the spectra are shown in dependence on the sample thickness for the LO sample. For the dominant mode in this part of the spectrum (denoted by capital A in the figure), it is clearly seen that the dependence of the frequency on the thickness significantly changes at the interface; while the first three removals of the coating result in pronounced increases of the resonant frequency of this mode, the difference between the last two spectra is relatively small. It is also seen that the width of this peak systematically increases with the increasing thickness of the coating; this indicates that internal friction of the coating becomes more and more dominant in damping of the vibration as the thickness of the coating increases. In Fig. 3, also a much smaller peak (B) can be seen. This mode was detectable only after the third removal and further. Nevertheless, the behavior of this mode is obviously different from the dominant one: its resonant frequency decreases steeply with the last removal (i.e. with the thickness of the substrate). In other words, Fig. 3 illustrates well that the subsequent reductions of the thickness of the specimen have measurable effects on the resonant frequencies

Table 1
Dimensions of the specimens; *a* is the dimension perpendicular to the substrate-coating interface, *b* and *c* are the in-plane dimensions.

	HO sample	LO sample
a [mm]	2.612	2.688
b [mm]	3.526	3.448
c [mm]	2.328	2.432
accuracy [mm]	±0.005	±0.005

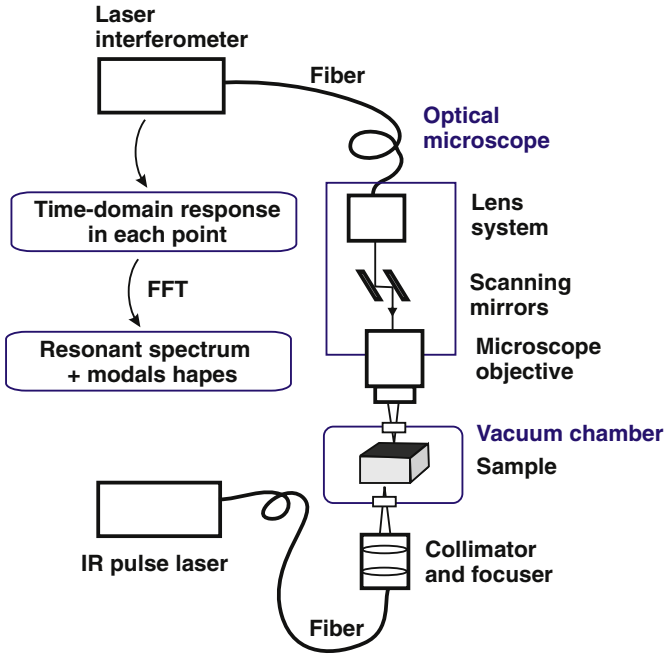

Fig. 2. Schematic outline of the contact-less RUS experimental set-up: the focused pulses from the IR laser generate elastic vibrations of a freely laid sample, these vibrations are recorded in individual point of the scanned surface by a laser interferometer through an optical microscope; the scanning is enabled by motorized mirrors; the signals recorded by the interferometer are processed by FFT to obtain the resonant spectrum and the modal shapes corresponding to the individual resonant peaks.

Table 2
Subsequent grinding of the coating — dimension a is the dimension perpendicular to the coating, HO and LO labels refer to high and low contents of oxides, respectively.

	HO sample thickness a [mm]	LO sample thickness a [mm]
Starting	2.612	2.688
After the 1st removal	2.530	2.594
After the 2nd removal	2.474	2.530
After the 3rd removal	2.397	2.453
After the 4th removal	2.205	2.309
After the 5th removal	2.122	2.211
Accuracy	±0.005	±0.005

and that these effects are different for different modes. Hence, it was proved that the effect of the coating material on the spectrum evolution with the thickness a is measurable, which justifies the construction of the direct and inverse problems described in the next subsection.

In addition to the RUS spectra measurements, the subsequent removals of thin layers also enabled determination of the density of both studied coatings. After each grinding, the weight of the sample was measured, and from the differences the values of density were obtained. There was no observable gradient in density across the thickness for any of the coatings, i.e. both coatings seemed to be homogeneous from this point of view. The results were: $\rho_{LO} = (6.73 \pm 0.39)\ \mathrm{g\cdot cm^{-3}}$and $\rho_{HO} = (6.82 \pm 0.25)\ \mathrm{g\cdot cm^{-3}}$, which indicates slightly higher porosity in the LO sample, as observed also in Fig. 1.

3.2. Direct and inverse problems

For the classical RUS measurements, the determination of the elastic coefficients from the experimentally obtained spectrum consists of two main parts: the direct and the inverse problem. The term direct problem stands for the calculation of the resonant frequencies of the used sample for given guesses of the elastic coefficients via a mathematical model; the term inverse problem then means iterative repetitions of the direct problem solution with successively refined guesses of the elastic constants until some optimal fit between the experimental and calculated spectra is reached.

In our modified case, we will use the term direct problem for the calculation of resonant spectrum evolution with the changing thickness a, providing that the geometry of the sample and the elastic constants and densities of both materials (substrate and coating) are known. For simplicity, we will assume that the thickness a ranges from the thickness of the substrate a_0 upward only, so we aim to calculate the evolution of the spectrum with increasing thickness of the layer.

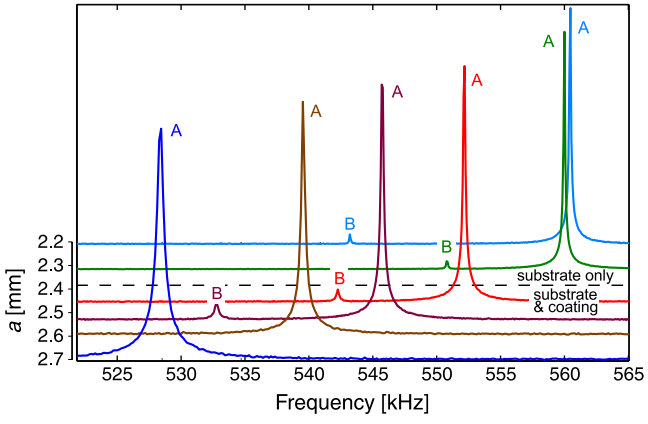

Fig. 3. Illustrative evolution of a part of the resonant spectrum of the LO sample with the successive removals of the coating. Capitals A and B denote two different modes (the latter visible for the first four spectra only), the straight dashed line separates the spectra obtained for the substrate only (i.e. after full removal of the coating) from those of the whole substrate-coating system.

Solution of this problem is equivalent to finding stationary points of the Lagrangian energy of harmonically vibrating substrate with a coating deposited on one of its faces for each given thickness a. These stationary points have the meanings of eigenfrequencies $\omega(a)$ and corresponding modal shapes $\mathbf{u}(\mathbf{x}, a)$. The required Lagrangian energy can be expressed as a sum of the Lagrangian energy of the substrate $\Lambda^{(s)}$ (independent of a) and the Lagrangian energy of the coating $\Lambda^{(c)}$ dependent of the coating thickness $a - a_0$, i.e.

$$\Lambda(a) = \Lambda^{(s)} + \Lambda^{(c)}(a - a_0), \tag{1}$$

where

$$\Lambda^{(s)} = \frac{1}{2}\int_{-a_0/2}^{a_0/2}\int_{-b/2}^{b/2}\int_{-c/2}^{c/2}\left(\rho^{(s)}\omega^2 u_i(\mathbf{x})u_i(\mathbf{x}) - C^{(s)}_{ijkl}\frac{\partial u_i}{\partial x_j}(\mathbf{x})\frac{\partial u_k}{\partial x_l}(\mathbf{x})\right) \times dx_1 dx_2 dx_3 \tag{2}$$

(ω is the angular frequency of vibrations, $\mathbf{u}(\mathbf{x})$ is the amplitude of the displacement field, $\rho^{(s)}$ is the density and $C^{(s)}_{ijkl}$ are the elastic coefficients of the substrate), and

$$\Lambda^{(c)} = \frac{1}{2}\int_{a_0/2}^{a-a_0/2}\int_{-b/2}^{b/2}\int_{-c/2}^{c/2}\left(\rho^{(c)}\omega^2 u_i(\mathbf{x})u_i(\mathbf{x}) - C^{(c)}_{ijkl}\frac{\partial u_i}{\partial x_j}(\mathbf{x})\frac{\partial u_k}{\partial x_l}(\mathbf{x})\right) \times dx_1 dx_2 dx_3 \tag{3}$$

($\rho^{(c)}$ and $C^{(c)}_{ijkl}$ are the density and the elastic coefficients of the coating, respectively).

In analogy to the classical RUS approach, one can find the stationary points by discretization of this energy in the sense of the Ritz–Rayleigh method, i.e. by taking the polynomial approximation of the displacement field amplitude in the substrate as

$$u_i(\mathbf{x}) = \sum_{k,l,m=1}^{N} \alpha_{klm,i} P_k\left(\frac{2x_1}{a_0}\right) P_l\left(\frac{2x_2}{b}\right) P_m\left(\frac{2x_3}{c}\right), \tag{4}$$

where $\mathbf{x} \in [-a_0/2; a_0/2] \times [-b/2; b/2] \times [-c/2; c/2]$, P_k denotes a normalized Legendre polynomial of the k-th order and $\alpha_{klm,i}$ are coefficients of the approximation. Then the Lagrangian energy of the substrate can be expressed by a quadratic form

$$\Lambda^{(s)}(\boldsymbol{\alpha}) = \frac{1}{2}\omega^2 \boldsymbol{\alpha}^{\mathrm{T}} \mathrm{M}^{(s)} \boldsymbol{\alpha} - \frac{1}{2}\boldsymbol{\alpha}^{\mathrm{T}} \mathbf{K}^{(s)} \boldsymbol{\alpha} \tag{5}$$

where $\boldsymbol{\alpha}$ is a column vector of coefficients $\alpha_{klm,i}$. The matrix $\mathbf{M}^{(s)}$ is diagonal and $\mathbf{K}^{(s)}$ is symmetric, positive semi-definite.

Similarly, the Lagrangian energy of the vibrating coating can be expressed as

$$\Lambda^{(c)}(\boldsymbol{\beta}) = \frac{1}{2}\omega^2 \boldsymbol{\beta}^{\mathrm{T}} \mathbf{M}^{(c)} \boldsymbol{\beta} - \frac{1}{2}\boldsymbol{\beta}^{\mathrm{T}} \mathbf{K}^{(c)} \boldsymbol{\beta}, \tag{6}$$

providing that the displacement field in the coating is approximated as

$$u_i(\mathbf{x}) = \sum_{k,l,m=1}^{N} \beta_{klm,i} P_k\left(\frac{2x_1 - a}{a - a_0}\right) P_l\left(\frac{2x_2}{b}\right) P_m\left(\frac{2x_3}{c}\right) \tag{7}$$

for $\mathbf{x} \in [a_0/2; a - a_0/2] \times [-b/2; b/2] \times [-c/2; c/2]$.

Without the coating ($a = a_0, \Lambda^{(c)} = 0$), the stationary points can be then found easily from the condition

$$0 = \nabla_\alpha \Lambda(\boldsymbol{\alpha}) = \left(\omega^2 \mathbf{M}^{(s)} - \mathbf{K}^{(s)}\right)\boldsymbol{\alpha}, \tag{8}$$

i.e. by solving a generalized eigenvalue problem. For a coating of non-zero thickness, the entire Lagrangian is

$$\Lambda(\boldsymbol{\alpha},\boldsymbol{\beta}) = \frac{1}{2}\omega^2 \begin{pmatrix} \boldsymbol{\alpha}^{\mathrm{T}} & \boldsymbol{\beta}^{\mathrm{T}} \end{pmatrix} \begin{pmatrix} \mathbf{M}^{(s)} & 0 \\ 0 & \mathbf{M}^{(c)} \end{pmatrix} \begin{pmatrix} \boldsymbol{\alpha} \\ \boldsymbol{\beta} \end{pmatrix} - \frac{1}{2} \begin{pmatrix} \boldsymbol{\alpha}^{\mathrm{T}} & \boldsymbol{\beta}^{\mathrm{T}} \end{pmatrix} \begin{pmatrix} \mathbf{K}^{(s)} & 0 \\ 0 & \mathbf{K}^{(c)} \end{pmatrix} \begin{pmatrix} \boldsymbol{\alpha} \\ \boldsymbol{\beta} \end{pmatrix}, \tag{9}$$

and its extrema must be sought under an additional constraint, ensuring the continuity of the displacement field at the substrate-coating interface. This constraint can be expressed by a linear condition on coefficients $\boldsymbol{\alpha}$ and β, i.e.

$$\mathbf{C}\begin{pmatrix} \boldsymbol{\alpha} \\ \boldsymbol{\beta} \end{pmatrix} = 0, \tag{10}$$

so the stationarity condition is

$$0 = \nabla_{(\alpha,\beta,\lambda)} \left[\Lambda(\boldsymbol{\alpha},\boldsymbol{\beta}) + \lambda \mathbf{C}\begin{pmatrix} \boldsymbol{\alpha} \\ \boldsymbol{\beta} \end{pmatrix} \right], \tag{11}$$

where λ is a Lagrangian multiplier, and $\Lambda(\boldsymbol{\alpha},\boldsymbol{\beta})$ is given in Eq. (9). Solution of this equation is then equivalent to solution of the eigenvalue problem

$$0 = \left[\omega^2 \begin{pmatrix} \mathbf{M}^{(s)} & 0 \\ 0 & \mathbf{M}^{(c)} \end{pmatrix} - \begin{pmatrix} \mathbf{K}^{(s)} & 0 \\ 0 & \mathbf{K}^{(c)} \end{pmatrix} \right] \begin{pmatrix} \boldsymbol{\alpha} \\ \boldsymbol{\beta} \end{pmatrix} \tag{12}$$

(analogous to Eq. (8)) in the null-space of the operator $\mathbf{C}$. If this is done for some chosen set of thicknesses $a > a_0$, the evolution of the resonant frequencies of the given sample with the thickness of the coating $\omega(a)$ is obtained. For $a < a_0$, the $\omega(a)$ dependence can be determined easily by solving the eigenvalue problem (8) with a used instead of a_0 in the approximation (4). By connecting these two curves together (they necessarily meet at $a = a_0$), the whole evolution of the resonant frequencies with the thickness of the sample can be calculated, running across the substrate-coating interface.

For the solution of the *inverse problem*, i.e. for the determination of the elastic modulus of the coating, it is necessary to repeat iteratively the solution of the direct problem until an optimal agreement between experimentally obtained and calculated $\omega(a)$ curves is reached. It is natural that this problem can be decomposed into two parts: determination of the elastic moduli of the substrate and, with the properties of the substrate already known, determination of the elastic moduli of the coating. The first step can be done by classical RUS approach, using the spectra obtained after the last (or the 4th) removal, when the whole sample contains only the substrate material. Since the substrate material is isotropic with only two independent elastic constants and has acceptably low internal friction (i.e. a high number of resonant modes can be detected and identified), this task is relatively simple.

For the second step of the inverse problem, it is necessary to make some assumptions on the elasticity of the coating and of the sensitivity of the RUS measurements to it. These assumptions are:

1. We assume that the material of the coating exhibits the so-called *transversely isotropic* symmetry with all in-plane directions being fully equivalent (the plane x_2x_3 is isotropic) and with five independent elastic coefficients c_{11}, c_{12}, c_{23}, c_{22} and c_{55}. This natural assumption follows from the symmetry of the spraying process; the effect of the lateral motion of the torch during spraying is considered as negligible.
2. We assume that the coating is sufficiently thin to be considered as mainly under plane-stress conditions. This means that (in some rough approximation) all mechanical loads imposed into the layer by the vibrations of the substrate are of dominantly in-plane nature, i.e. consisting of in-plane tension/compressions and in-plane shears only. The two-dimensional elasticity of a thin layer under the plane-stress condition can, in general, characterized by a two-dimensional 4th order tensor q_{IJKL} such that [28]:

$$\sigma_{IJ} = \sum_{K,L\in\{2,3\}} q_{IJKL}\varepsilon_{KL} \tag{13}$$

(considering x_1 as the direction perpendicular to the layer; no Einstein's summation law applied for indices denoted by capital letters). It can be shown (e.g. [40]) that the tensor q_{IJKL} for the transversely isotropic layer has only two independent components, which are

$$q_{2222} = c_{22} - \frac{c_{12}^2}{c_{11}} \tag{14}$$

and

$$q_{2323} = \frac{(c_{22} - c_{23})}{2}. \tag{15}$$

Hence, it is assumed that the RUS measurements themselves are insufficient for accurate determination of other elastic coefficients c_{ij} than the combinations given by q_{2222} and q_{2323}. To obtain information on the full anisotropy of the coating, some complementary measurements are necessary. This is analogous to the case of RUS applied to bulk materials, where the determination of all independent elastic coefficients requires sometimes the RUS measurement to be complemented by measurements of the longitudinal wave velocities in direction perpendicular to the faces of the sample [38,33]. Such velocities are related to the elastic constants c_{ij} via the Christoffel's equation (e.g. [39]), which means that these complementary results can be used as constraints for the calculation of elastic constants from the RUS spectrum, as will be shown later.

Since there are five sought elastic coefficients and RUS can provide only two combinations of them, three complementary measurements are necessary. If there can be thin free-standing samples prepared from the coating, two more elastic constants can be easily obtained by pulse-echo or through-transmission [41] measurements (one longitudinal and one shear wave velocity in the direction perpendicular to the coating). To overcome the problem with the high internal friction, the thickness of this free-standing sample can be reduced by grinding until the echoed or transmitted ultrasonic pulse is reliably detectable. On the other hand, if the coating is thick enough (e.g. ~1 mm as in our case), also a small free-standing sample can be used for measurements of the longitudinal velocity in the in-plane direction. In addition, such sample can be used also for measurements of velocities of two shear modes in the in-plane direction (shear modes with in-plane and out-of-plane polarizations), which would provide two more values, possibly usable as independent verification of the results. However, it must be taken into account that one of these in-plane shear velocities is the same as the out-of-plane shear velocity (following from the symmetry of the material), so only one additional constraint for the inverse calculation would be obtained.

Under these two assumptions, the inverse problem for the coatings can be formulated by finding the minimum of some objective function (the superscripts exp. and calc. denote the experimentally determined values and the calculated ones, respectively)

$$F(c_{kl}) = \sum_{i,j} \left[\omega_i^{\mathrm{exp}}\left(a_j\right) - \omega_i^{\mathrm{calc}}\left(a_j, c_{kl}\right) \right]^2 + \gamma \sum_{i,j} \left[v_i^{\mathrm{exp}} - v_i^{\mathrm{calc}}(c_{kl}) \right]^2, \tag{16}$$

$$kl \in \{11, 12, 23, 22, 55\},$$

where $a_j > a_0$ are all thicknesses of the sample during the successive removals of the coating material, $\omega_i(a_j)$ denotes the resonant frequency of the i-th mode for each such thickness, v_i are velocities determined by the complementary measurements, and γ is a weighting factor. The mutual association between the experimentally obtained

resonant frequencies (ω_i^{exp}) and their calculated counterparts (ω_i^{calc}) is done based on the similarity of their modal shapes.

3.3. Estimation of the effective thickness of the substrate

Before applying the above described inverse procedure to the experimental spectra for the LO and HO samples, it is necessary to discuss one more possible source of inaccuracy of the measurement: as seen in the micrographs in Fig. 1, the interface between the coating and the surface is not exactly planar, which is a result of substrate grit-blasting necessary to obtain sufficient adhesion of the coating to the substrate. The interface is rather wavy, with the bottom-to-peak difference up to approximately 80 μm, which is comparable to the thicknesses of the layers removed during each of the first three repetitions of the experimental procedure. However, the numerical model for the solution of the direct problem described in Section 3.2 requires an exact knowledge of the value a_0, i.e. of the interface position. For this reason, some estimation of the effective thickness of the layer must be done. Such estimates are enabled by the fact that the whole region influenced by the wavy interface was fully removed during the fourth grinding (removed thickness ≳150 μm), so the third and the fifth removals correspond purely to changes of the thickness of the coating and of the substrate, respectively.

In [28], the shifts of the frequencies induced by the presence of the layer were studied by various numerical models. It was shown that for thin layers the shifts are linearly proportional to the thickness of the layer and that this approximation can be used with acceptable accuracy up to ratios $\log[(a - a_0)/a_0] < -1.5$. This means that this approximation could be also utilized for some rough estimates of the changes of the spectrum during the third and the fifth removals ($\Delta a < 100$ μm), at least for the lowest few modes for which the wavelengths of the modal shapes (given by the dimensions of the samples, i.e. ~2 mm) are much longer than the thickness of the removed layer. Hence, we can estimate the effective position of the substrate-layer interface as shown in Fig. 4: it can be assumed that the frequency of each mode changes linearly with the thickness a in the vicinity of the interface, and that the slope of this dependence changes abruptly at the interface as the material properties change there. Thus, if two linear extrapolations are constructed, one for the third removal (in the coating) and one for the fifth removal (in the substrate), the effective position of the interface is located in the point where these two extrapolations intersect. As seen in Fig. 4, the intersection points for the first three modes for the LO sample all fall within a narrow interval; the mean value of the location of the intersection points can be then taken as the effective position of the interface.

By using this approach and with the experimental inaccuracy in the determination of the resonant frequencies (±1 kHz) taken into account, the effective thicknesses of the substrate were obtained as $a_0^{LO} = (2.340 \pm 0.020)$ mm and $a_0^{HO} = (2.260 \pm 0.020)$ mm (which means that the initial thicknesses of the coatings were 348 μm and 352 μm, respectively), taking the three modes shown in Fig. 4 for the LO sample and also the first three modes for the HO sample. These values of a_0 were the used for all calculations of the $\omega(a)$ curves. Let us mention that the real $\omega(a)$ curves are probably rather smooth, changing their slopes continuously throughout the interfacial region. Nevertheless, as it will be seen in the next section, our model with a sharp, effectively localized interface gives a good agreement with the discrete experimental data $\omega_i^{exp}(a_j)$. From another point of view, by using this approach only the frequency shifts induced by removing of pure (substrate or coating) materials are effectively involved in inverse calculation of the elastic constants, as the $\omega(a)$ curve in the $[a_3, a_4]$ interval is approximated by linear extrapolations of the neighboring intervals, so the effect of the real structure of the interface on the results is, in some sense, suppressed.

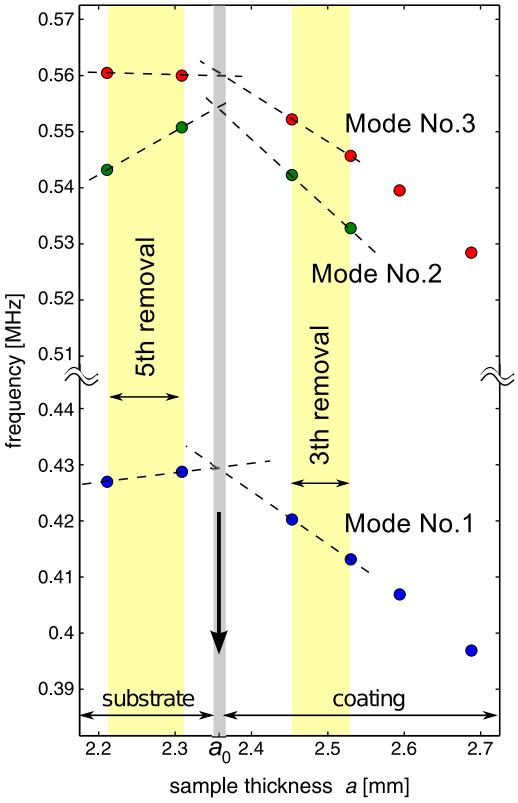

Fig. 4. Estimation of the effective thickness of the coating from the intersections of linear extrapolations of $\omega(a)$ curves.

4. Results and discussion

4.1. Optimized elastic constants

Following the scheme outlined in Section 3.2, the elastic constants of both substrates were first determined. On this purpose, 25 modes were identified in the last spectrum (after the 5th grinding) for each sample and these modes were then used for the inverse calculation. The results were $c_{11}^{LO} = (284.5 \pm 0.3)$ GPa, $c_{44}^{LO} = (84.3 \pm 0.2)$ GPa, $c_{11}^{HO} = (284.2 \pm 0.3)$ GPa, and $c_{44}^{HO} = (84.1 \pm 0.2)$ GPa, which agrees well with the fact that the materials of both substrates were identical. Then, thirteen resonant modes were chosen for each sample that was easily identifiable both for the substrate and for the coating. According to the modal shapes, it was carefully checked that each of the chosen resonant peaks corresponds to the same mode along the whole experimentally obtained $\omega(a)$ curve.[1] For this input set of $\omega_i^{exp}(a_j)$, the inverse problem was solved by minimizing the objective function (16). To obtain the complementary data, a 600 μm thick free-standing sample was prepared from each coating, and the ultrasonic through-transmission method was applied to measure the phase velocities of longitudinal (L) elastic waves v_L and shear (T) elastic waves v_T in the out-of-plane directions. The results were

$$v_{L,x_1}^{LO} = (2.91 \pm 0.02)\,\mathrm{mm \cdot \mu s^{-1}}, \tag{17}$$

$$v_{T,x_1}^{LO} = (1.61 \pm 0.02)\,\mathrm{mm \cdot \mu s^{-1}}, \tag{18}$$

[1] As only one face of the sample is scanned by the laser-Doppler interferometry and as only one component of the displacement field of this face is obtained, two modes of quite different modal shapes may appear to be similar or indistinguishable from the experimental data (see for example modes Nos. 1 and 4 in Fig. 5). To avoid the possible incorrect association in such cases, all admissible identifications were tried, and it was checked that only one of them enables acceptable agreement between the experimentally obtained and optimized theoretical $\omega(a)$ curves.

$$v_{L,x_1}^{HO} = (3.51 \pm 0.02)\text{mm}\cdot\mu\text{s}^{-1}, \quad (19)$$

$$v_{T,x_1}^{HO} = (2.10 \pm 0.02)\text{mm}\cdot\mu\text{s}^{-1}, \quad (20)$$

(the measurements were done at 2 MHz for the longitudinal waves and at 2.5 MHz for the shear waves). Further, the same method was applied to determine the in-plane velocity of the longitudinal mode with the result:

$$v_{L,x_2}^{LO} = (3.03 \pm 0.08)\text{mm}\cdot\mu\text{s}^{-1}, \quad (21)$$

$$v_{L,x_2}^{HO} = (3.71 \pm 0.08)\text{mm}\cdot\mu\text{s}^{-1}. \quad (22)$$

The shear wave velocities in this direction were not measurable. A strong damping was observed, which (together with significant dispersion, probably due to both the microstructure of the coating and the small lateral dimension of the sample) disabled any reliable detection of the arrival times of the pulses. Nevertheless, as discussed in Section 3.2, three additional measurements for each sample should be sufficient for complementing the RUS data. The fact that these shear wave velocities were not determinable by the through-transmission measurements due to strong damping illustrates well the advantage of the RUS concept described in this paper; while the attenuation is so strong that the traveling waves cannot propagate through even a relatively thin free-standing sample, the vibrations of the substrate are detectable and carry the sought information on the properties of the coating.

The obtained velocities were then used for the joint inverse procedure based on minimization of the objective function (16), with the weighting factor taken as $\gamma = V^{-1/3}$, where V is the volume of the free-standing sample. (This choice of the weighting coefficient γ ensures that the individual velocities are involved with the same weight as through-thickness resonant modes of a cube with the same volume as the real sample, so the velocity data are scaled to be comparable with the RUS resonant frequencies.) The results are summarized in Table 3 (upper part). It is clearly seen that all elastic constants are higher for the HO coating, which confirms the results of the 4 PB tests. Also the anisotropic character of the coatings is obvious: the in-plane longitudinal moduli (c_{22}) are in both cases higher than the out-of-plane ones (c_{11}). The same is true for the shear moduli: the shearing along the splats (c_{55}) is elastically softer than the shearing perpendicular to them (c_{44}). To illustrate the anisotropy, it is possible also to recalculate the elastic constants into the in-plane Young's modulus (E_2) and the out-of-plane Young's modulus (E_1), which are given in the middle part of Table 3. The ratios $\alpha = E_1/E_2$ are relatively high, at least compared with the results obtained by Tan et al. [24] for single-phase coatings; this is in agreement with the fact that with the lower content of the oxides (the LO sample), this ratio decreases, i.e. the presence of the oxides leads to isotropization of the coating.

For comparison, two additional numbers are given in the middle part of Table 3: the bulk moduli K and the in-plane Young's moduli determined by the four-point bending tests E_2^{4PB}. The bulk moduli illustrate how strongly the sprayed material is elastically weakened compared with bulk steels (K ~ 160 GPa). The decrease by more than 70% cannot be ascribed solely to the porosity and the corresponding decreased density; the low value of K rather indicates that the interconnections between the individual components of the coatings (splats, oxide layers) are poor.

As far as the results of the four-point bending tests are concerned, it is clearly seen that at high (ultrasonic) frequencies and for very small strain amplitudes (~10^{-6}), the materials of both coatings behave as significantly elastically stiffer than under static bending loads with strain amplitudes up to 0.05%. This means that the elastic responses of the coatings in the bending tests are effectively softened by viscous, relaxation-like processes (e.g. mutual splat sliding) and/or nonlinearity resulting from high amplitudes (e.g. opening/closing of microcracks and pores) that are not affecting the elasticity of the coatings in the ultrasonic regime. Moreover, even so small straining of the coating may lead to localized failure of splat bonds and formation of microcracks [42,43] due to inhomogeneous microstructure of the coating. Nevertheless, the results of both methods are in agreement with the fact that the HO coating is significantly elastically stiffer.

Table 3
Elastic constants of the studied WSP coatings. Upper part: full anisotropic tensors; middle part: engineering constants (Young's and bulk moduli) and the comparison with the results of the four-point bending tests; lower part: chosen components of the compliance tensor s_{ij}. The experimental errors were determined by Monte-Carlo simulations, taking into account both the different sensitivities of the measurements with respect to individual elastic coefficients (the sensitivity analysis was carried out according to [38]) and the uncertainties in the density of the coatings under study.

	LO sample	HO sample
c_{11} [GPa]	56.9 ± 3.4	83.5 ± 3.2
c_{22} [GPa]	61.8 ± 3.2	93.2 ± 3.3
c_{55} [GPa]	17.4 ± 1.4	30.3 ± 1.6
c_{12} [GPa]	23.8 ± 6.1	27.5 ± 8.4
c_{23} [GPa]	9.7 ± 5.3	24.3 ± 5.0
c_{44} [GPa][a]	26.0 ± 2.1	34.5 ± 2.2
E_1 [GPa]	41.3 ± 9.5	70.6 ± 8.2
E_2 [GPa]	51.8 ± 4.7	81.4 ± 3.5
$\alpha = E/E$	0.79 ± 0.10	0.87 ± 0.09
K [GPa]	32.6 ± 3.8	47.6 ± 5.3
E_2^{4PB} [GPa]	28 ± 7	45 ± 9
S_{12} [GPa^{-1}]	$(-8.1 \pm 3.0) \cdot 10^{-3}$	$(-3.3 \pm 1.6) \cdot 10^{-3}$
S_{23} [GPa^{-1}]	~0[b]	$(-2.2 \pm 1.0) \cdot 10^{-3}$

[a] Calculated as $(c_{22} - c_{23})/2$.
[b] The value of S_{23} calculated from the elastic tensor c_{ij} is $-7.7\,10^{-5}$ GPa^{-1}, which is by more than an order of magnitude smaller than the experimental accuracy $\pm 2.3 \cdot 10^{-3}$ GPa^{-1}.

The agreement between the calculated and experimental $\omega(a)$ curves is seen in Fig. 5 for the LO sample and in Fig. 6 for the HO sample: in both cases the model follows well the experimental curves with the maximal misfit of 12 kHz (approximately 1.5%) and with most of the misfits smaller than 5 kHz. We can conclude that the numerical model used within the forward problem is able to predict well the evolution of the resonant frequencies with thickness of the coating for the resulting values of the elastic coefficients. Similarly, for the resulting set of elastic coefficients also the wave velocities measured on the free-standing samples were fitted with error smaller than 1%, which is comparable with the experimental accuracy of the through-transmission method. This agreement between the calculated and experimental $\omega(a)$ curves in the whole measurement range also confirms that the behavior of the whole coating can be well described by one set of elastic constants, i.e. that there are no detectable differences between the materials removed within the subsequent steps. This indicates that the studied coatings were macroscopically homogeneous, and that the grinding and polishing in the individual steps of the experimental procedure did not affect significantly their properties.

4.2. Degeneracy of the elastic tensor

Let us now discuss the relation between the obtained elastic tensors and the microstructures of the coatings. As follows from the analysis by Sevostianov and Kachanov [1], the anisotropy of some plasma sprayed coatings is dominantly given by an oriented array of microcracks, which leads to the so-called *elliptic* degeneracy of the elastic tensor, and possible reduction of the number of independent elastic coefficients (see [1,34] for more details). For the coatings under study, this

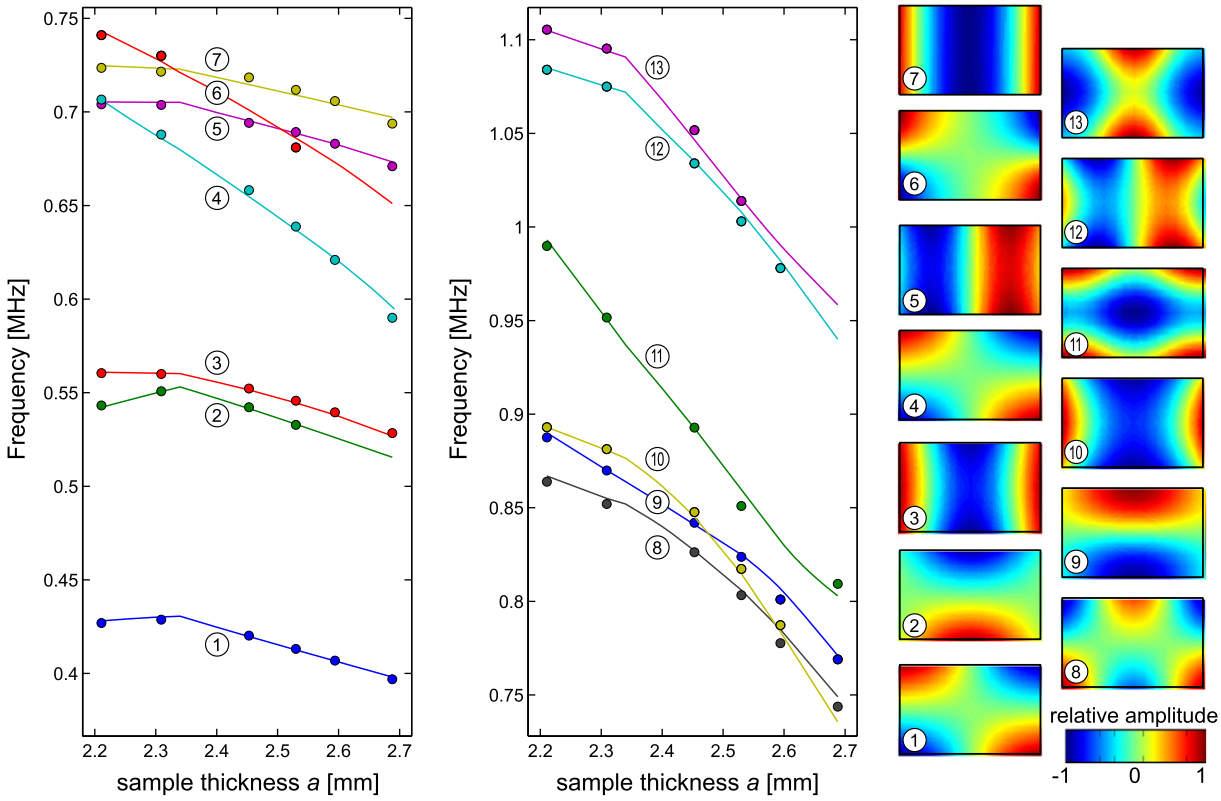

Fig. 5. Agreement between experimental and optimized $\omega(a)$ curves for the LO sample. Solid lines are the calculated curves, full circles are the experimental values of resonant frequencies. Maps on the right show the (calculated) modal shapes corresponding to the thirteen used modes, numbered consecutively as 1,...,13 (numbers in the circles).

model is probably not fully realistic, since their anisotropy is also influenced by the shapes of the splats and the oxidic layers along the splat boundaries. Nevertheless, such microstructure can be, again, understood as an oriented array of defects, in this case of the splat-to-oxide interfaces, so it is meaningful to discuss whether the degeneracy appears.

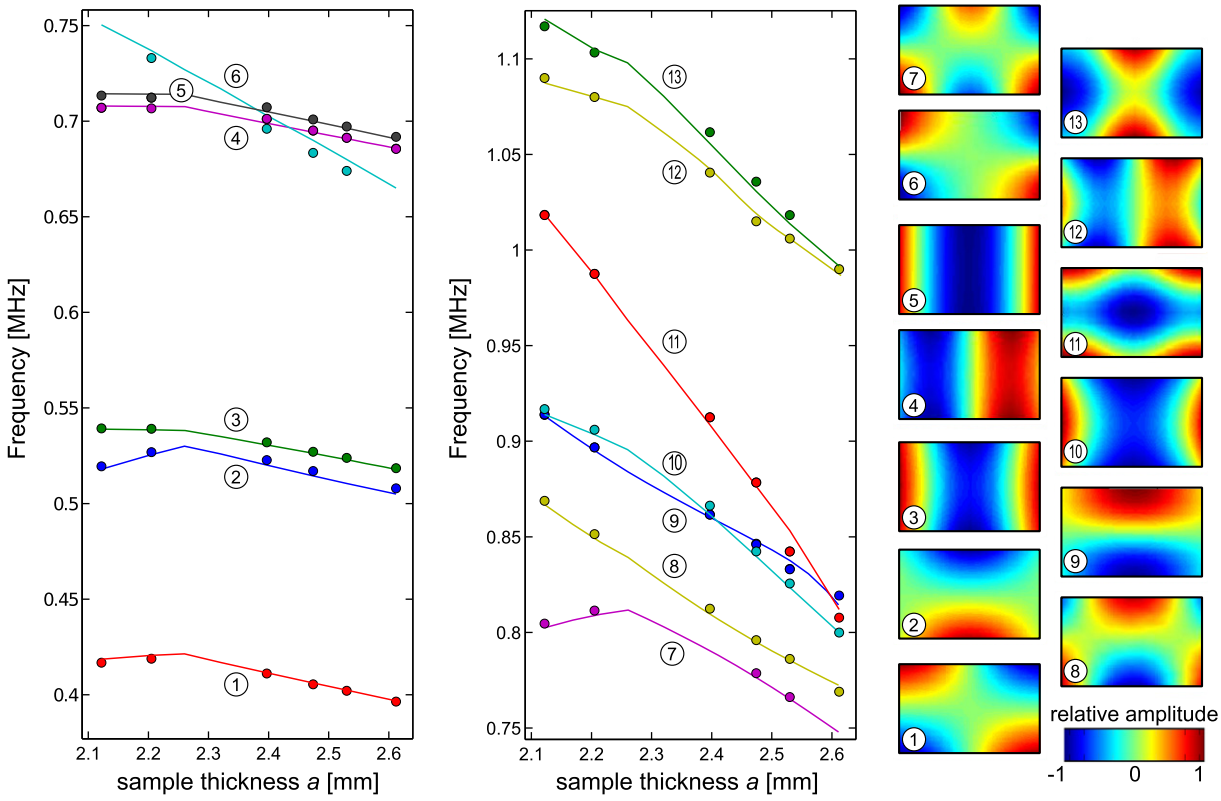

Fig. 6. Agreement between experimental and optimized $\omega(a)$ curves for the HO sample; notation is the same as in Fig. 5.

Two levels of degeneracy are possible for a transversely isotropic medium [34]:

1. if the anisotropy is induced by an oriented array of (arbitrary, spheroid-like) defects, the directional dependence of a square root of the Young's modulus ($\sqrt{E}$) is an ellipse; this adds one algebraic condition on the elastic constants and reduces the number of the independent ones from five to four.
2. if these defects are micro-cracks, an additional degeneracy appears, since then

$$s_{12} = s_{23}, \tag{23}$$

where s_{ij} is the matrix inverse to c_{ij}; the number of independent constants is reduced from four to three.

In Fig. 7, the polar plots of experimentally determined Young's moduli are seen (the dots) in comparison with the elliptic fits (solid lines)

$$E = \left(\sqrt{E}\right)^2 = \left[\sqrt{E_1}\cos(\vartheta) + \sqrt{E_2}\sin(\vartheta)\right]^2, \tag{24}$$

where ϑ is an angular coordinate with $\vartheta = 0$ aligned with the x_1 axis. Obviously, the curves are in a perfect agreement; we can conclude that the first condition is satisfied and both coatings indeed exhibit an elliptic form of elasticity with only four independent elastic coefficients.

The values of the compliance coefficients s_{12} and s_{23} are seen in Table 3 (the lower part). It is obvious that the condition for degeneracy is not fulfilled for the LO sample, where the values of these two coefficients differ by two orders of magnitude. For the HO sample, the difference is smaller, comparable with the experimental error, but still pronounced enough to indicate that the second condition is rather not satisfied. We can conclude that the anisotropy of both coatings, although being of elliptic type, cannot be ascribed to the array of microcracks. Thus, four independent elastic coefficients are sufficient for the description of the elasticity of the examined coatings, but further reduction of this number to three is impossible.

In addition to the discussion of the degeneracy of the elastic tensor, the values of s_{ij} given in Table 3 enable also some deeper insight into the micromechanics of the coatings, and, consequently, a better explanation of the difference between the HO and LO samples. It is seen that the compliance coefficient s_{23} is anomalously small for the LO coating, and significantly smaller than s_{12} for the HO coating. This coefficient represents the in-plane shrinking of the material when an in-plane tensile load (in a perpendicular direction) is applied. The fact that this coefficient is small reveals that there are very weak interconnections between the individual splats in the in-plane directions; this might be a consequence of, for example, microcracks oriented perpendicular to the coating plane. For the HO sample, the coating microstructure seems to provide more efficient mutual bonding of the splats. On the other hand, the out-of-plane interconnections (coefficient s_{12}) seem to be stronger for the LO sample. This phenomenon may be explained by different characters of the splat interfaces namely their shape and presence of pores and oxides along them (see Fig. 2) providing different levels of mutual mechanical interlocking and physical bonding of the splats.

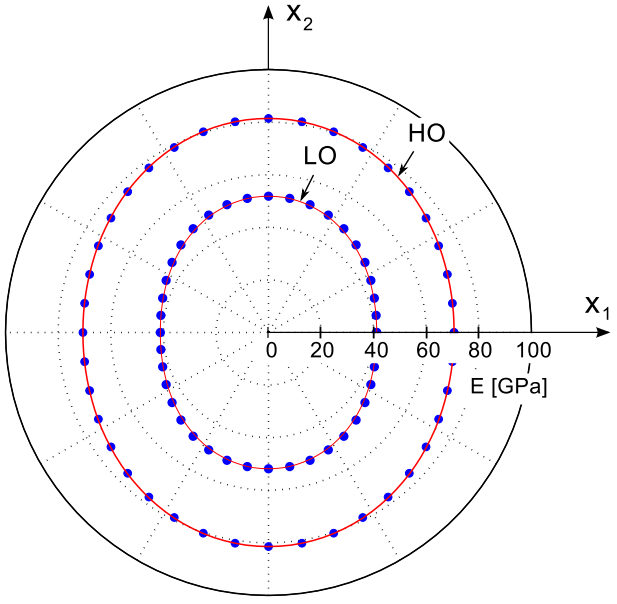

Fig. 7. Directional dependence of the Young's moduli for both samples; dots are values calculated from the optimized elastic coefficients c_{ij}, solid lines are elliptic approximations (24).

4.3. Internal friction analysis

As seen in Fig. 3, the high internal friction of the coating leads to progressive broadening of the resonant peaks in the spectrum with increasing thickness a. Besides this qualitative observation, the evolution of the widths of the peaks with a enables also a quantitative estimation of the internal friction of the coating. For such analysis, we will assume that the effective width of each peak is a function of two quantities: the internal friction of the substrate ($Q_{(s)}^{-1}$), which is given by the complex part of the shear modulus of the substrate, and the internal friction of the coating ($Q_{(c)}^{-1}$), which is given by the complex part of the shear modulus of the coating. For simplicity, we take the coating in this case as isotropic, with only one shear modulus and only one shear coefficient of the internal friction. For a homogeneous sample of an isotropic material, the resonant spectra are dependent on both two independent elastic coefficients (the shear modulus G and the bulk modulus K, for example). However, the lowest few resonant frequencies correspond mainly to shearing modes, so they are dominantly dependent on G, while their sensitivity to K is weaker, as it can be shown by the sensitivity analysis described in [38]. Here, we assume, for simplicity, similarly strong dependence of the first few resonant frequencies of the heterogeneous, sandwich-like sample on the shear moduli of the substrate and of the coating only, with their dependence on the bulk moduli fully neglected.

For the substrate, the value $Q_{(s)}^{-1}$ can be directly determined from the FWHM/f ratios (FWHM stands for full width at half maximum, f is the resonant frequency) of the chosen nine peaks from the spectrum after the last (fifth) grinding. The resulting values are: $Q_{(s),\mathrm{LO}}^{-1} = (0.42 \pm 0.04) \cdot 10^{-3}$ and $Q_{(s),\mathrm{HO}}^{-1} = (0.40 \pm 0.05) \cdot 10^{-3}$, which corresponds well to the fact that the materials of both substrates were identical.

With the value of $Q_{(s)}^{-1}$ known, the internal friction coefficients of the coating ($Q_{(c)}^{-1}$) were determined by using the perturbation approach described in [36,37]. In this approach, it is assumed that the effective internal friction on the p-th resonant peak $Q_p^{-1} = \mathrm{FWHM}_p/f_p$ is the function of the shear moduli $G_{(s)}$ and $G_{(c)}$ and of the internal friction coefficients $Q_{(s)}^{-1}$ and $Q_{(c)}^{-1}$ of the substrate and of the coating, respectively. Under such assumption, and considering that $Q_{p,(c,s)}^{-1} \ll 1$, it can be shown that [36]

$$Q_p^{-1} = \frac{2}{f_p}\left(\frac{\partial f_p}{\partial G_{(s)}} G_{(s)} Q_{(s)}^{-1} + \frac{\partial f_p}{\partial G_{(c)}} G_{(c)} Q_{(c)}^{-1}\right), \tag{25}$$

where the partial derivatives can be obtained from the solution of the direct problem.

It is clearly seen that this relation is easily invertible, i.e. the value of $Q_{(c)}^{-1}$ can be calculated from known values of $Q_{(s)}^{-1}$ and the FWHM/f ratios for the experimentally obtained resonant peaks. This was done for all those peaks used for the inverse calculation of the elastic constants in Section 4.1 with the results listed in Table 4. It can be concluded that there is no pronounced difference between the internal frictions of the LO and HO coatings, as the average values are very close to each

other. In general, the damping in the coating is at least 10 times higher than in the substrate, which agrees well with the fact that plasma spraying leads to a significant increase of damping capacity of steel substrates [35].

As seen in Table 4 and in Fig. 8, there are some differences in the $Q_{(c)}^{-1}$ values obtained for different thicknesses of the coatings. However, these differences are comparable with the experimental errors, so any discussion of their origin would be unjustified. It can be only concluded that there is no steep increase or decrease of $Q_{(c)}^{-1}$ across the thickness of the coating, as all obtained values are at least of the same order of magnitude.

5. Conclusions

The main aim of this paper was to present a modification of resonant ultrasound spectroscopy for evaluation of plasma sprayed coatings with high internal friction. As the damping capacity of such coatings does not allow them to be analyzed by RUS in the free-standing state, the coatings in this modification are used in the as sprayed state, i.e. supported by substrates, and their properties are extracted from the evolution of the RUS spectra of the substrates during successive removal of the coatings. As seen from the results obtained for two different WSP coatings, such method can be used for accurate determination of the elastic constants of the coatings (when complemented by through-transmission measurements, a full anisotropic tensor is obtained), and also some rough estimates of the internal friction. The outputs of this method enable a discussion of the anisotropic elasticity of the examined coatings and its possible degeneracy. For our case of steel WSP coatings, it was shown that the ellipticity condition for $\sqrt{E}$ is satisfied, so the elastic anisotropy is determined by four independent elastic coefficients only.

Since the frequencies in ultrasonic methods are high and the loading amplitudes extremely low, the in-plane Young's moduli obtained by the proposed method are much stiffer than those determined for the same materials by four-point bending tests, where the elastic response is effectively softened by inelastic and relaxation-like phenomena. Similar discrepancy would probably appear also between our results and results of any other quasi-static tests, such as nanoindentation. Thus, it is obvious that although the proposed method is relatively time-consuming and rather complicated as far as the post-processing of the data is concerned, it can provide valuable data complimentary to conventional techniques. This method surely requires further experimental verifications (i.e. application to coatings prepared by different spraying methods and for different materials of both the substrate and the coating); nevertheless, the results obtained so far are very promising and indicate that further development of ultrasonic methods for characterization of supported plasma-sprayed coatings may be justified and meaningful.

Acknowledgment

This work has been supported by the Czech Science Foundation (grants nos. 107/13-13616S, 101/09/0702, P108/12/1872 and P108/12/P552), the Academy of Sciences of the Czech Republic (project M100761203 and the institutional support No. RVO:61388998) and the SGS program of the Czech Technical University (project no. OHK4-002/13).

Table 4
Internal friction parameters of the studied coatings as determined for various thicknesses: before the first removal of the coating ($j = 0$) and successively after three removals until the substrate-coating interface was reached ($j = 1,2,3$).

j (number of removals)	LO sample		HO sample	
	$(a_j - a_0)$ [μm] (coating thickness)	$Q_{(c)}^{-1}$ [10^{-3}]	$(a_j - a_0)$ [μm] (coating thickness)	$Q_{(c)}^{-1}$ [10^{-3}]
3	113	6.00 ± 3.98	134	6.16 ± 2.65
2	190	5.73 ± 2.83	211	5.60 ± 1.57
1	254	8.25 ± 2.41	267	7.34 ± 1.82
0	348	10.76 ± 4.10	352	9.68 ± 1.88
	Average	7.69 ± 3.98		7.19 ± 3.38

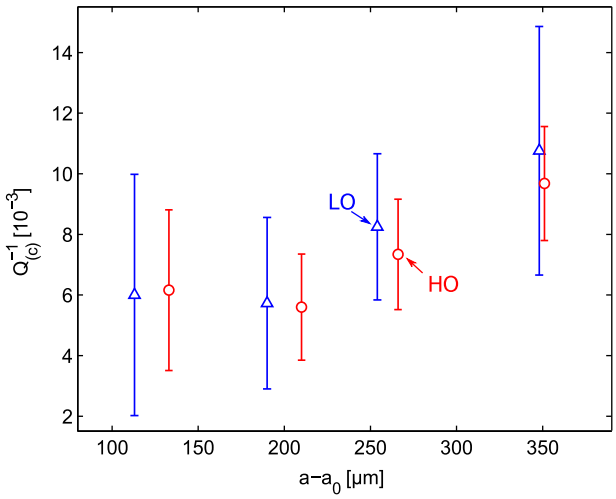

Fig. 8. Evolution of the average internal friction parameter $Q_{(c)}^{-1}$ with the thickness of the coating.

References

[1] I. Sevostianov, M. Kachanov, Acta Mater. 48 (2000) 1361–1370.
[2] R.S. Lima, B.R. Marple, Acta Mater. 52 (2004) 1163–1170.
[3] J. Matějíček, S. Sampath, Acta Mater. 51 (2003) 863–872.
[4] J. Matějíček, S. Sampath, D. Gilmore, R. Neiser, Acta Mater. 51 (2003) 873–885.
[5] J. Zhu, H. Xie, Z. Hu, P. Chen, Q. Zhang, Surf. Coat. Technol. 206 (6) (2011) 1396–1402.
[6] H.J. Kim, Y.G. Kweon, Thin Solid Films 342 (1999) 201–206.
[7] A. Rico, J. Gómez-García, C.J. Múnez, P. Poza, V. Utrilla, Surf. Coat. Technol. 203 (2009) 2307–2314.
[8] E. Raón, V. Bonache, M.D. Salvador, J.J. Roa, E. Sánchez, Surf. Coat. Technol. 205 (2011) 4192–4197.
[9] E. Rayón, V. Bonache, M.D. Salvador, E. Bannier, E. Sánchez, A. Denoirjean, H. Ageorges, Surf. Coat. Technol. 206 (2012) 2655–2660.
[10] F. Kroupa, J. Therm. Spray Technol. 16 (2007) 84–95.
[11] J. Malzbender, R.W. Steinbrech, J. Mater. Res. 18 (2003) 1975–1984.
[12] W.Z. Wang, C.J. Li, Y.Y. Wang, G.J. Yang, K. Sonoya, Surf. Coat. Technol. 201 (2006) 842–847.
[13] F. Azarmi, T. Coyle, J. Mostaghimi, Surf. Coat. Technol. 203 (2009) 1045–1054.
[14] R. Mušálek, O. Kovářík, J. Matějíček, Surf. Coat. Technol. 205 (2010) 1807–1811.
[15] R. Mušálek, J. Matějíček, M. Vilémová, O. Kovářík, J. Therm. Spray Technol. 19 (1–2) (2010) 422–428.
[16] P. Strunz, G. Schumacher, R. Vassen, A. Wiedenmann, Acta Mater. 52 (2004) 3305–3312.
[17] J. Pina, A. Dias, J.L. Lebrun, Mater. Sci. Eng., A A267 (1999) 130–144.
[18] S. Parthasarathi, B.R. Tittmann, K. Sampath, E.J. Onesto, J. Therm. Spray Technol. 4 (1995) 367–373.
[19] R.J. Damani, A. Wanner, J. Mater. Sci. 35 (2000) 4307–4318.
[20] H.P. Crutzen, F. Lakestani, J.R. Nicholls, IEEE Ultrasonics Symp., 1997, pp. 657–660.
[21] H.P. Crutzen, F. Lakestani, J.R. Nicholls, Ultrasonic Characterisation of Thermal Barrier Coatings, IEEE Ultrasonics Symp., 1996, pp. 731–734.
[22] R. Lima, S. Kruger, G. Lamouche, B. Marple, J. Therm. Spray Technol. 14 (2005) 52–60.
[23] A. Portinha, V. Texeira, J. Cerneiro, M.G. Beghi, C.E. Bottani, N. Franco, R. Vassen, D. Stoever, A.D. Sequeira, Surf. Coat. Technol. 188–189 (2004) 120–128.
[24] Y. Tan, A. Shyam, W.B. Choi, E. Lara-Curzio, S. Sampath, Acta Mater. 58 (2010) 5305–5315.
[25] A. Migliori, J.L. Sarrao, W.M. Visscher, T.M. Bell, M. Lei, Z. Fisk, R.G. Leisure, Physica B 183 (1993) 1–24.
[26] N. Nakamura, H. Ogi, M. Hirao, Ultrasonics 42 (2004) 491–494.
[27] L. Yu, Y. Ma, C. Zhou, H. Xu, Mater. Sci. Eng., A 407 (2005) 174–179.
[28] M. Růžek, P. Sedlák, H. Seiner, A. Kruisová, M. Landa, J. Acoust. Soc. Am. 128 (2010) 3426–3437.
[29] T. Lauwagie, K. Lambrinou, S. Patsias, W. Heylen, J. Vleugels, NDT&E Int. 41 (2008) 88–97.
[30] V. Harok, K. Neufuss, J. Therm. Spray Technol. 10 (2001) 126–132.
[31] P. Sedlák, M. Landa, H. Seiner, L. Bicanová, L. Heller, Proceedings of the 1st International Symposium on Laser Ultrasonics: Science, Technology and Applications, The e-Journal of Nondestructive Testing, Kirchwald, 2008, (www.ndt.net).

[32] D.H. Hurley, et al., J. Appl. Phys. 107 (2010), (art. no. 063510).
[33] H. Seiner, et al., Acta Mater. 58 (2010) 235–247.
[34] I. Sevostianov, M. Kachanov, Int. J. Eng. Sci. 46 (2008) 211–223.
[35] B.A. Potekhin, S.G. Lukashenko, S.P. Kochugov, Met. Sci. Heat Treat. 42 (2000) 407–410.
[36] Y. Sumino, I. Ohno, T. Goto, M. Kumazawa, J. Phys. Earth 24 (1976) 263–273.
[37] R.G. Leisure, F.A. Willis, J. Phys. Condens. Matter 9 (1997) 6001–6029.
[38] M. Landa, P. Sedlák, H. Seiner, L. Heller, L. Bicanová, P. Šittner, V. Novák, Appl. Phys. A 96 (2009) 557–567.
[39] M.J.P. Musgrave, Crystal Acoustics, Holden Day, San Francisco, 1965.
[40] R.M. Jones, Mechanics of Composite Materials, McGraw-Hill, New York, 1975.
[41] M. Levy, H. Bass, R. Stern, Handbook of Elastic Properties of Solids, Liquids, and Gases, vol. 1, Academic Press, New York, 2000.
[42] R. Mušálek, V. Pejchal, M. Vilémová, J. Matějíček, J. Therm, Spray Technol. 22 (2013) 221–232.
[43] M. Vilémová, J. Matějíček, R. Mušálek, J. Nohava, J. Therm. Spray Technol. 21 (2012) 372–382.